# Atomic photoionization in a changing plasma environment

T. N. Chang[1] and T. K. Fang[2,*]

[1]*Department of Physics and Astronomy, University of Southern California, Los Angeles, California 90089-0484, USA*

[2]*Department of Physics, Fu Jen Catholic University, Taipei, Taiwan 242, Republic of China*

(Received 27 April 2013; published 5 August 2013)

We present a detailed theoretical study on the photoionization of one- and two-electron atoms subject to an external changing plasma environment based on the Debye-Hückel model. Specifically, by examining the migration of the bound excited states into the continuum in the presence of plasma, our investigation has led to resonancelike photoionization structures immediately above the ionization thresholds for H, $H^-$, and He atoms. For He, unlike the usual Fano-Beutler resonances due to the configuration mixing between the doubly excited components and the single ionization channel with different $\ell_1\ell_2$ angular momenta combinations in the final-state wave function, these plasma-induced resonancelike structures result from the mixing of the quasibound and continuum components of the same $\ell_1\ell_2$ combination in the final-state function. With a number of specific examples, we show that the general features of these spectra could be linked directly to the overlap at small $r$ between the effective wave functions of the outgoing ionized electron and the atomic electron in its initial states.

DOI: 10.1103/PhysRevA.88.023406 PACS number(s): 32.80.Fb, 32.80.Gc, 32.30.Jc, 52.25.Os

## I. INTRODUCTION

Recent theoretical studies of atomic processes in a plasma environment [1–10] have attracted considerable interest following a number of earlier works [11–13] based on the application of the Debye-Hückel model [14] for a classical electron-ion collisionless plasma under thermodynamic equilibrium. Nearly all such theoretical estimations [1–10] were carried out with a screened Coulomb potential $V_s$ (or the Yukawa potential) for an atomic electron in the vicinity of a nuclear charge $Z$ subject to a one-electron Hamiltonian, i.e.,

$$h_o(r;D)=\frac{p^2}{2m}+V_s(r;D) \quad \text{and} \quad V_s(r;D)=-\frac{Ze^2}{r}e^{-r/D}, \tag{1}$$

where $p$ is the momentum of the electron and the parameter $D$ is known as the Debye-Hückel length (or Debye length). The Debye length characterizes the screening of the nuclear charge experienced by the atomic electron due to the plasma in the outer region of an atom and is given in units of Bohr radius, $a_0$, by (see also, e.g., Eq. (2.5) of [13])

$$D=1.304\times10^8(T/n)^{1/2}a_0, \tag{2}$$

where $T$ and $n$ are the plasma temperature (in degrees Kelvin) and density (in $\mathrm{cm}^{-3}$), respectively. Or, alternatively, it can be expressed in units of cm by $D=6.90(T/n)^{1/2}$. The value of $D$ ranges over many orders of magnitude, i.e., from $1\times10^{-2}$ nm for the plasma in a solar core to over $1\times10^4$ m for the ones in an intergalactic medium. Since the plasma temperature usually varies only three to four orders in magnitude (e.g., from $1\times10^2$ to $1\times10^6$ K), the value of $D$ (or the degree of penetration of the ion-electron gas into the atom) depends more on the variation of the plasma density.

For low-density plasmas such as the ones in an interstellar medium or even for those generated in low-power gas discharge, the Debye length $D$ may be a few orders of magnitude larger than the size of the atoms and should have little effect on the atomic processes. Since the plasma frequency of an electron (i.e., $\omega_p\sim n^{1/2}$) is also relatively small and the period of plasma oscillation is substantially longer than the time scale of a typical atomic process, the plasma environment effect on atomic transition is also expected to be minimal. On the other hand, for a high-density plasma system such as the ones in the sun and sunlike stars, the Debye length is of the order of $10^{-11}$ m. Consequently, the effect of the Debye screening could change significantly the atomic transitions for the astrophysically relevant elements. That, in turn, could have substantial implication for the *opacity* data, which is of critical importance to the development of high-quality equation-of-state models for such systems [15]. In fact, both the commonly applied equation-of-state models, MHD (Mihalas-Hummer-Däppen) and OPAL (Opacity Project at Livermore), include the leading Coulomb correction (i.e., the Debye-Hückel term) to ideal-gas thermodynamics in the current standard solar models [16].

Following the Debye-Hückel original approximation, the potential $V_o(r)$ due to an electron-ion plasma at a distance $r$ far from a force center (e.g., an atomic nucleus) outside an inner Debye sphere of radius $A$ can be derived from Gauss' law

$$\nabla^2V_o(r)=-\frac{\rho(r)}{\epsilon_p}, \quad r\geqslant A, \tag{3}$$

where $\epsilon_p$ is the dielectric constant of the electron-ion gas and $\rho$ is its total charge density at $r$. Assuming a charge density of $\rho_o$ at $r=\infty$ with a zero potential $V_o(r=\infty)=0$ and following the Boltzmann distribution, the charge densities of the positive charge $q$ and the negative charge $-q$ at $r$ could be expressed as $\rho_+(r)=\rho_o e^{-qV_o(r)/\kappa T}$ and $\rho_-(r)=\rho_o e^{+qV_o(r)/\kappa T}$, respectively, where $\kappa$ is the Boltzmann constant and $T$ the absolute temperature. The net total charge density at $r$ is then given by

$$\rho(r)=\rho_o\left(e^{-\frac{qV_o(r)}{\kappa T}}-e^{\frac{qV_o(r)}{\kappa T}}\right)=-2\rho_o\sinh\left(\frac{qV_o(r)}{\kappa T}\right). \tag{4}$$

*051420@mail.fju.edu.tw

 

Assuming, in addition, that the potential energy is relatively small compared to the kinetic energy, Eq. (3) for the potential $V_o(r)$ in the outer region of the Debye sphere could then be approximated by the *linear* Poisson-Boltzmann equation,

$$\nabla^2 V_o(r) = \left(\frac{1}{D^2}\right) V_o(r), \quad r \geqslant A, \tag{5}$$

where $D > A$ is the Debye length given by Eq. (2) and defined in terms of the charge density $n(\sim q\rho_o)$ and the temperature $T$ outside the Debye sphere. The potential inside the Debye sphere can also be derived from Gauss' law and takes the form of

$$V_i(r) = -\frac{Ze}{r} + \text{const}, \quad r \leqslant A, \tag{6}$$

with a nucleus charge $Z$ located at $r = 0$. By matching the two potentials $V_o$ and $V_i$ and their first-order derivatives at $r = A$, one gets [12,13]

$$V_s(r; D) = \begin{cases} V_i(r) = -Ze^2\left(\frac{1}{r} - \frac{1}{D+A}\right), & r \leqslant A, \\ V_o(r) = -Ze^2\left(\frac{De^{A/D}}{D+A}\right)\frac{e^{-r/D}}{r}, & r \geqslant A. \end{cases} \tag{7}$$

In the limit when $A \to 0$, Eq. (7) reduces approximately to the screened Coulomb potential employed in most of the recent theoretical atomic calculations. Clearly, the Debye model breaks down when $D \to A$. An alternative screened Coulomb potential for Debye screening with four parameters was introduced by Wang and Winkler [8] in their theoretical calculation. For the one-electron atom, the most interesting feature resulting from the screened Coulomb potential is the disappearance of the bound state as $D$ becomes smaller than the corresponding *critical screening length* of that particular state (see, e.g., Tables III and IV of [11]). In other words, the potential can only attract a decreasingly finite number of bound states below the ionization threshold as $D$ decreases [11–13]. We should point out that any estimate of the plasma effect on atomic process based on the Debye-Hückel model should be limited to Debye lengths that are sufficiently longer than the radius $A$ of the inner Debye sphere, i.e., the average size of the plasma-free atoms.

In addition to the solar plasma discussed earlier, for the laser-produced dense plasma at an electronic temperature of a few hundred eV and a density of $1 \times 10^{22}$ to $1 \times 10^{24}$ cm$^{-3}$ [17,18], the Debye length would be comparable to the size of the atoms. Although the laser-produced plasma is far from a thermodynamically equilibrium system, a detailed theoretical estimate based on the Debye-Hückel model may help to better understand the physics behind the observed spectra, particularly the shift of the spectral lines. Qualitatively, the shift in energy levels due to the increase in plasma density (or as $D$ decreases) would then lead to a redshift in the resulting spectral lines in the emission spectrum. Indeed, such shifts were observed in the laser-produced high-density plasmas near the surface of the solid graphite targets [17].

An equally interesting question would then be what happens to the bound-bound transitions (i.e., the emission lines) when the upper excited states move into the continuum. Some of the recent studies on photoionization and electron-atom impact ionization have led to a fairly general feature, i.e., the presence of a narrow resonancelike structure immediately above the ionization threshold and its transformation to a broad continuum structure as the Debye length decreases, or when the plasma effect increases [4,5]. This general feature was attributed plausibly either as the shape resonance or as a transformation of Feshbach resonance into shape resonance. It is also interesting to note that there is a sharp increase of the cross sections from a value of zero at the threshold to the peak cross section, in contrast to the known monotonically decreasing photoionization cross sections for plasma-free hydrogen as energy increases [19]. It is the main purpose of this paper to show that such features could be easily and directly linked to the overlap of the effective one-electron wave functions between the bound electron initially and the outgoing electron in the continuum. We also present in detail the migration of the photoionization spectra of two-electron systems such as He and $H^-$ and show that the absence of a bound excited state for plasma-free $H^-$ will lead to spectra that are very different from the resonancelike structures for H or He.

## II. PHOTOIONIZATION OF ONE-ELECTRON ATOM

By using the discretized $B$-spline-based atomic orbits, the photoionization cross section $\sigma$ from an initial state $I$ to a final continuum $F$ with an outgoing electron of momentum $k$ could be expressed in terms of the oscillator strength $f_{FI}$ by the expression [20,21]

$$\sigma = \frac{4\pi\alpha}{kA_o^2} f_{FI}, \tag{8}$$

where $\alpha$ is the fine structure constant and $A_o$ is the amplitude of the outgoing one-electron oscillating wave function. We should note that the usual per-unit energy normalization constant $(2/\pi k)^{1/2}$ is replaced by $A_o$ for the $B$-spline-based atomic wave functions confined in a sphere of radius $R$. For the one-electron atoms, the one-particle radial wave functions $\chi_{v\ell}(r)$ subject to the potential $V_s$, in the form of either Eq. (1) or Eq. (7), are generated by the one-electron Hamiltonian given by Eq. (1); i.e.,

$$h_o(r; D)\chi_{v\ell} = \epsilon_{v\ell}\chi_{v\ell}, \tag{9}$$

where $\ell$ is the orbital angular momentum and $\epsilon_{v\ell}$ is the energy eigenvalue. For the outgoing ionized electron, $v$ represents the energy $\epsilon = k^2$ in rydbergs. The oscillator strength $f_{FI}$ and its corresponding photoionization cross section are determined by the one-electron dipole radial matrix $\langle \chi_{n\ell} \mid d \mid \chi_{k\ell'} \rangle$ of the dipole operator $d$, either in length or velocity approximation, between the wave functions of the initial state $\chi_{n\ell}$ and the final state $\chi_{k\ell'}$. Qualitatively, it is clear that the greater the overlap between $\chi_{n\ell}(r)$ and $\chi_{k\ell'(r)}$, the larger the cross section. In the present calculation, the numerical accuracy of our calculation is ensured as the length and velocity results of the cross section are in agreement to four digits or better.

Figure 1 presents our theoretical results on the variation of the hydrogen photoionization spectra corresponding to the $1s \to 4p$ transition as the Debye length decreases from the critical screening length of the $4p$ state, which is slightly greater than $25a_0$. We have chosen the migration of the $1s \to 4p$ transition as our example to ensure that the range

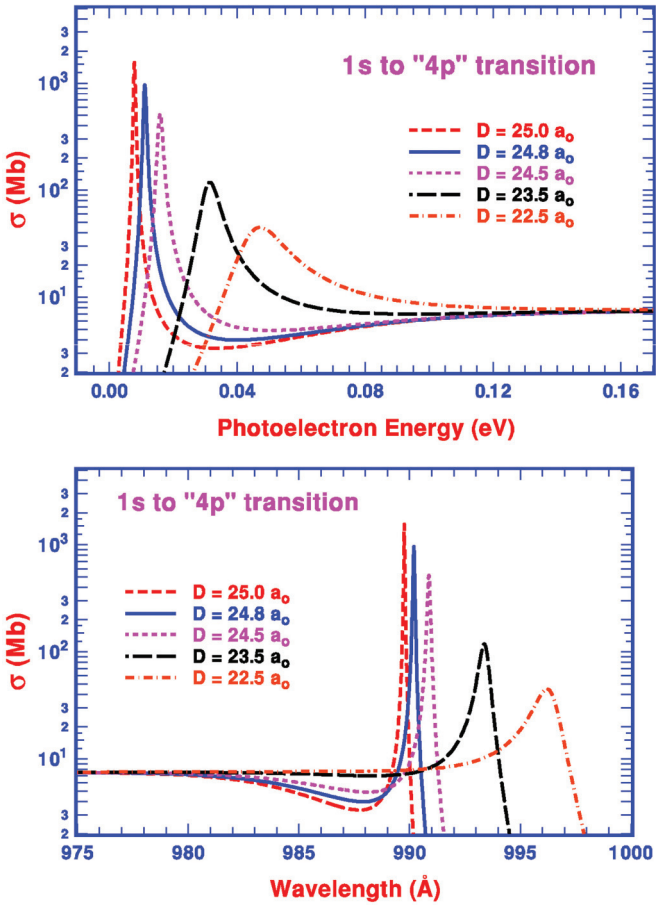


FIG. 1. (Color online) Hydrogen photoionization spectra corresponding to $1s \rightarrow 4p$ transition as $D$ varies with $A = 0$.

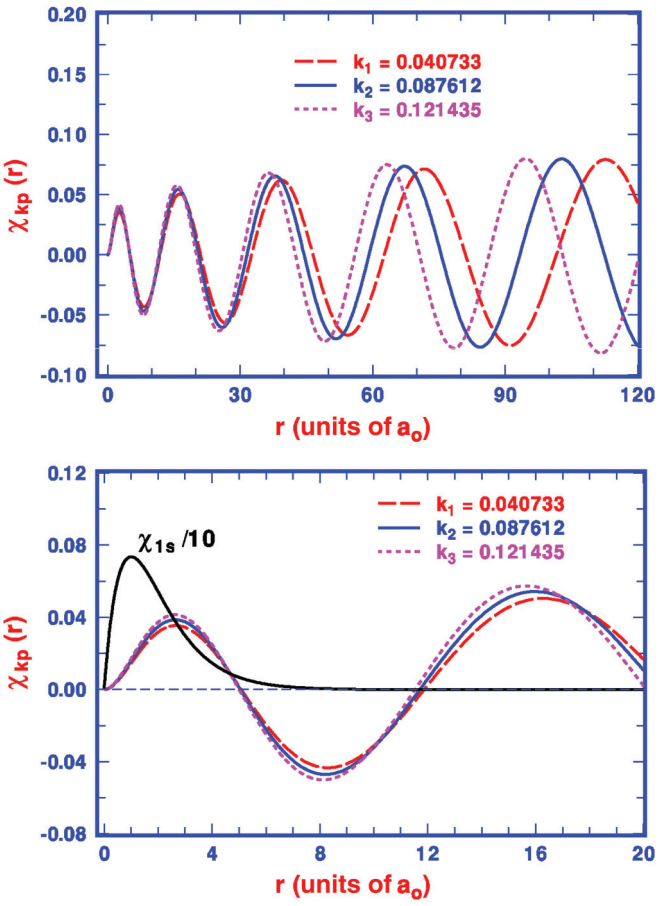


FIG. 2. (Color online) The radial wave functions $\chi_{kp}$ of the outgoing ionized electron of the plasma-free hydrogen at a number of momenta. The bottom plot compares $\chi_{kp}$ with $\chi_{1s}$ wave function (reduced by a factor of 10) of the initial $1s$ orbit at small $r$ (in units of $a_0$).

of the Debye lengths is sufficiently large compared to the size of the hydrogen atom in its $1s$ ground state, so that the Debye-Hückel model is a reasonable approximation to emulate the outside plasma environment. The top plot of Fig. 1 confirms the general feature suggested by the recent theoretical results [4,5] discussed earlier, i.e., from a narrow resonancelike structure at a $D$ value close to the critical screening length to a broad continuous spectrum as $D$ decreases. The bottom plot of Fig. 1 shows the redshift from the $4p \rightarrow 1s$ emission line, now in terms of a narrow resonancelike absorption line near 989.5 Å as the $4p$ state moves into the continuum due to the increase of the plasma effect. This shift is significant compared to the corresponding plasma-free Lyman-$\gamma$ line at 972.5 Å.

For a plasma-free hydrogen atom, the radial part of the one-particle wave functions at small distance $r$ from the nucleus for the outgoing $kp$ electron are essentially the same until they are sufficiently away from the nucleus. The top plot of Fig. 2 shows such wave functions at a number of momenta $k$. As expected, they all reach their first local maxima and the subsequent zeros at about the same values of $r$ as shown. In other words, the penetration of the wave functions at small $r$ depends little on the energy (or momentum) of the outgoing electron. For photoionization, the difference in the $kp$ wave functions at large distance, in fact, has little effect on its cross section. The slight difference in the first loop of the wave functions and its overlap with the wave functions of the initial $1s$ electron (with its maximum at $r = a_0$ shown in the bottom plot of Fig. 2) dictate entirely the photoionization spectrum. Consequently, as we pointed out earlier, the photoionization spectrum for plasma-free hydrogen is known to decrease monotonically as the energy increases [19]. We note that the wave functions shown in Fig. 2 and all subsequent figures are plotted against the radial distance $r$ from the nucleus in units of Bohr radius, $a_0$.

For the screened Coulomb potential with $D = 24.5a_0$ (i.e., at a $D$ value slightly less than the critical screening length for the $4p$ state), the radial wave functions shown in Fig. 3 for the outgoing electron at energies near the threshold behave very differently from that shown in Fig. 2. Although the local maxima and their subsequent zeros for the first loop of all three wave functions $\chi_{kp}$ near the origin stay at the same $r$ as the ones shown in Fig. 2, their magnitudes are substantially different as $k$ increases. At $k = 0.014953$, the magnitude of its first loop is almost zero, representing a very small penetration of the ionized electron into the inner region of the atom due to its relatively small kinetic energy. At a slightly higher energy near $k = 0.034244$, our calculation leads to a quasibound radial wave function with a relatively small amplitude for the outside oscillating wave function. As the energy increases further, $\chi_{kp}$ with $k = 0.053371$ behaves more like the plasma-free

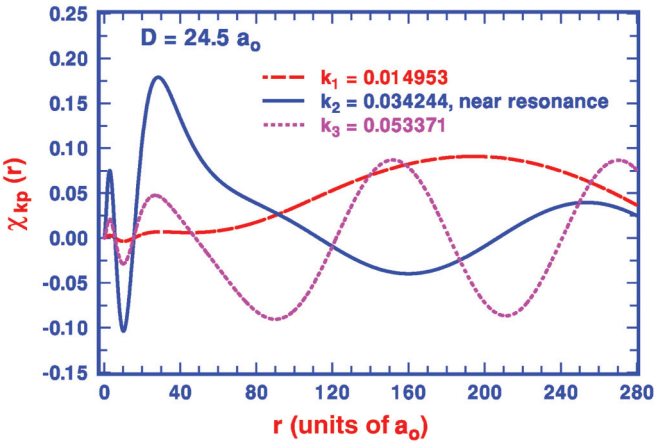


FIG. 3. (Color online) The radial wave function $\chi_{kp}$ of the outgoing ionized electron of hydrogen with $D = 24.5a_0$ at a number of momenta.

ones shown in Fig. 2. Since the radial wave function of the initial $1s$ electron is mostly confined at $r$ less than $5a_0$, the dipole matrix element is essentially determined by the overlap between the first loop of the $\chi_{kp}$ and $\chi_{1s}$. Therefore, with a magnitude of near-zero first loop at $k = 0.014953$, it is easy to conclude a near-zero threshold cross section as shown in Fig. 1. As the energy increases to that for the quasibound state at $k$ close to 0.034244, the overlap between $\chi_{kp}$ and $\chi_{1s}$ is at its maximum and thus the peak of the sharp narrow resonancelike structure appears. At even higher energy when the radial wave functions behave like the plasma-free atom, a monotonically decreasing cross section such as the one shown in Fig. 1 is expected. Our calculation shows a progressively more diffused quasibound radial wave function with decreasing $D$, thus, the broadening of the resonancelike structure. Eventually, the narrow resonancelike structure evolves into a continuous spectrum as shown in Fig. 1. Our explicit example also leads to the conclusion that the dynamics of the photoionization is short range in nature and depends mostly on the size of the atom in its initial state.

## III. PHOTOIONIZATION OF TWO-ELECTRON ATOM

For the multielectron atoms (e.g., $H^-$, He, and Li), a number of recent works [3,6–8] appear to suggest that many of the singly excited states remain bound even when $D$ is smaller than the average size of an isolated atom in the same singly bound excited states. In particular, for the ground state of $H^-$, it concludes that, even when $D$ is substantially smaller than the average size of the ground state of the isolated $H^-$, its ground state remains bound [7]. Such an implication is intuitively and qualitatively different from the migration of the bound states into the continuum for the hydrogen atoms in a plasma environment. This qualitative disparity between the disappearance of the bound states in one- and two-electron atoms may have resulted from an *a priori* application of the Debye screening to the electron-electron interaction in the form of

$$V_{ij} = \frac{e^2}{r_{ij}} e^{-r_{ij}/D}, \tag{10}$$

where $r_{ij}$ is the distance between the atomic electrons. It has effectively led to a potential between the atomic electrons that is significantly more attractive than it should be by reducing greatly the Coulomb repulsion between atomic electrons, thus, leaving the atom in a bound state even when $D$ is smaller than the average size of an isolated atom in that particular bound state.

The less attractive nature of the screened Coulomb potential for an atomic electron in the field of the nuclear charge $Z$ could be understood easily since, close to the atomic nucleus, there is a non-negligible presence of the free-moving electrons from the plasma outside with their relatively high mobility. However, to justify a similar Coulomb screening between two atomic electrons would require an unlikely qualitative picture, i.e., a substantial presence of the positive ions between atomic electrons, in spite of the relatively low mobility for the much heavier ions. In addition, since the screened potentials discussed above are derived from Gauss' law by assuming a stationary nuclear charge $Z$ located at $r = 0$, a similar approach could not be applied directly to the free-moving atomic electrons. In other words, there is no compelling reason to modify the electron-electron interaction by the same Coulomb screening.

For the charged-particle (e.g., proton) impact excitation of hydrogenlike atomic systems in a plasma environment, the interaction between the incident particle and the atomic electron is long range in nature either before or after the collision. Scheibner *et al.* [22] proposed two different static potentials to treat such processes for (1) the low-temperature and high-density plasmas and (2) the high-temperature and low-density plasmas, respectively. The Debye screening in their calculation was included only between the incident charged particle and the target nucleus. Since the dynamics of the atomic photoionization is essentially short range in nature, together with the lack of theoretical ground to include the Debye screening in the electron-electron interaction between atomic electrons as we discussed earlier, the $N$-electron Hamiltonian for an atom in a plasma environment in our photoionization calculation is expressed in terms of $h_o(r; D)$, given in Eq. (1) as

$$H(r_i, r_j, \ldots; D) = \sum_{i=1,N} h_o(r_i; D) + \sum_{i>j}^{N} \frac{e^2}{r_{ij}}, \tag{11}$$

where $r_{ij} = |\vec{r}_i - \vec{r}_j|$ represents the separation between the atomic electrons $i$ and $j$. The one-particle Hamiltonian $h_o$ for the individual atomic electron is subject to a potential $V_s$ given by either the Yukawa potential or the one from Eq. (7). The numerical results presented below are calculated with the $B$-spline-based configuration interaction (BSCI) method which has been applied successfully to a large number of atomic structure properties. Details of the theoretical approach, the computation procedures, and a large number of its applications have already been presented elsewhere [20,21]. The initial and final states of the photoionization are calculated typically with a basis set of atomic orbitals representing over 10 000 two-electron configurations. The calculated photoionization cross sections in length and velocity approximations agree to at least three digits or better. One of the advantages of the BSCI approach is its ability to map out

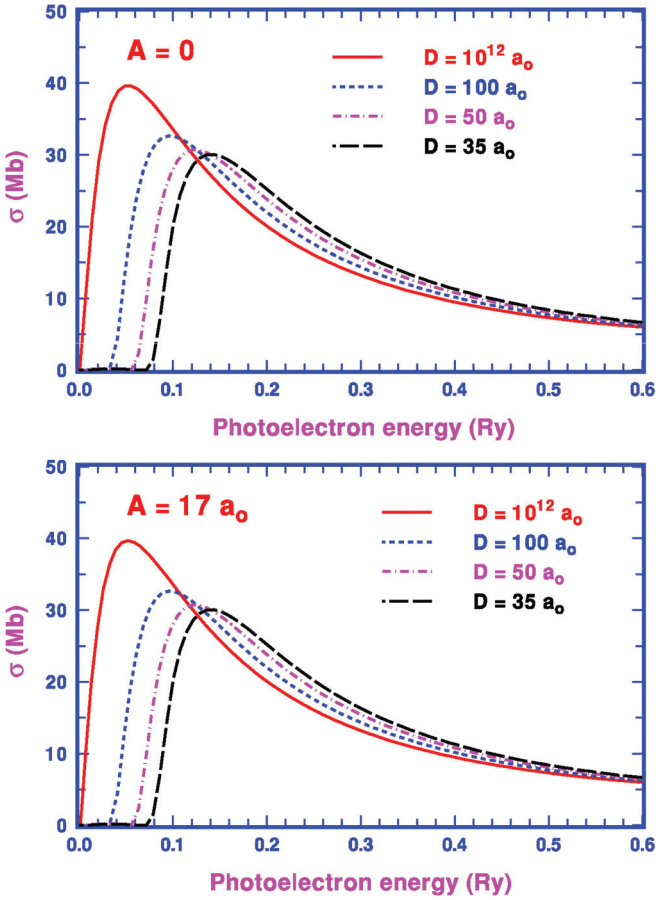


FIG. 4. (Color online) $H^-$ photoionization spectra with $A = 0$ and $A = 17a_0$ as $D$ varies.

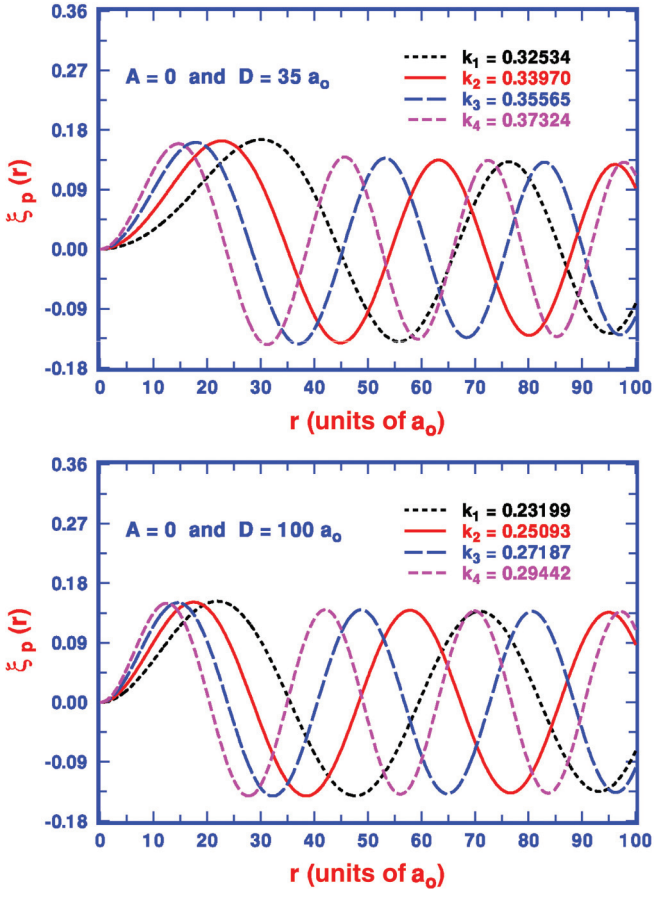


FIG. 5. (Color online) The effective radial wave functions $\xi_p$ of the outgoing ionized electron of $H^-$ with $D = 35a_0$ and $D = 100a_0$ at a number of momenta.

the configuration-mixed effective one-electron wave function $\xi_\ell(r)$ (see Eq. (50) of [20]) of the photoionized outgoing electron. By examining explicitly this effective one-electron outgoing wave function, we are able to analyze qualitatively the general feature of the photoionization spectra for the two-electron atoms similar to what we did earlier for the hydrogen atom.

For $H^-$, with only one bound state, the migration of the bound-bound transition into a narrow resonancelike structure in the continuum near the ionization threshold is not expected. Indeed, Fig. 4 shows the absence of such a resonancelike structure as $D$ decreases from the plasma-free $H^-$ at $D = \infty$. The top plot in Fig. 4 presents the calculated spectra using the Yukawa potential and the bottom plot shows the ones using the potential given by Eq. (7) with a nominally assigned value of $A = 17a_0$ (i.e., about the size of $H^-$ in its ground state). Except for a minor quantitative difference, the general feature is nearly the same in how the spectra evolve as $D$ varies. A careful inspection of the spectra indicates a near-zero cross section for photoelectrons with kinetic energy up to about 0.075 Ry (i.e., about 1 eV) for the spectrum with $D = 35a_0$. Even at greater value of $D$, e.g., at $D = 100a_0$, the cross section remains near zero from the threshold until the kinetic energy of the photoelectron increases to about 0.35 eV.

Figure 5 presents the configuration-mixed effective wave functions $\xi_p$ for the outgoing photoionized $p$ electron at a number of momenta. The top plot shows that at $D = 35a_0$ the first local maximum of $\xi_p$ shifts outward at a fairly rapid rate as the momentum $k$ decreases. In fact, at $k = 0.32534$ (i.e., at a photoelectron energy about 1.4 eV), the first local maximum is already located at $r$ greater than $30a_0$, i.e., at a distance from the origin at about twice the size of the $H^-$ in its ground state. In other words, the overlap between the wave functions of the outgoing electron and the electron in its initial state is relatively small. Clearly, the cross section, which is proportional to the square of the dipole matrix element, would decrease even faster as the overlap of the wave functions decreases rapidly when the momentum decreases, thus resulting in a near-zero cross section at an energy less than 1 eV as shown. On the other hand, the penetration of the ionized electron to the smaller $r$ region also increases substantially at slightly higher momentum, thus resulting in a fast rise in cross section at energy higher than 1 eV. With substantially less Debye screening at $D = 100a_0$, the bottom plot of Fig. 5 shows that the penetration of the outgoing electron to the small-$r$ region is stronger than the ones at $D = 35a_0$, even when the photoelectron is less energetic. Consequently, the onset of the sharp rise in photoionization cross section occurs much closer to the threshold at around 0.35 eV. This threshold feature of the photoionization spectra is very different from that for the hydrogen atom subject to a plasma environment, where the photoionization cross section starts its sharp increase at the threshold without any shift.

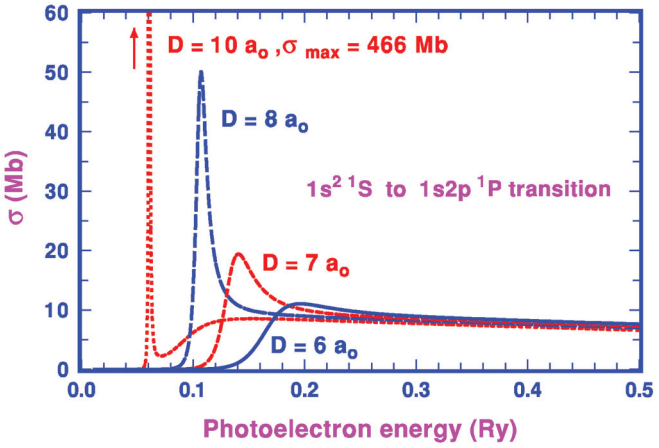


FIG. 6. (Color online) He photoionization spectra corresponding to $1s^2\,{}^1S \rightarrow 1s2p\,{}^1P$ transition as $D$ varies with $A = 0$.

Qualitatively, this difference in the threshold feature could be accounted for by the presence of the second atomic electron in $H^-$. The presence of the remaining electron in the photoionization of $H^-$ has the effect of reducing the probability density of the low-energy outgoing electron in the small-$r$ region due to the Coulomb repulsion between electrons. Since the screened Coulomb potential has the effect of increasing the average radius of the atomic orbit of the remaining electron, the reduction of the probability density of the ionized electron at small $r$ would be greater with a smaller $D$. Therefore, it requires more kinetic energy of the outgoing electron to penetrate into the inner region of the atom for a more appreciable overlap between the initial and final orbits. This is exactly what happens when the sharp rise of the photoionization spectrum from the near-zero cross section occurs at around 0.35 eV with $D = 100a_0$, whereas with $D = 35a_0$, it starts at around 1 eV.

For the He atom, with its two electrons and a large number of strong bound-bound transitions similar to the hydrogen atom, one could readily conclude that its photoionization spectra would have the general features similar to the ones we discussed earlier. Figure 6 shows our theoretical results of the migration of the photoionization spectra corresponding to the $1s^2\,{}^1S \rightarrow 1s2p\,{}^1P$ transition with decreasing Debye length from $10a_0$ to $6a_0$. Indeed, the change from the narrow resonancelike structures into broad continuum spectra is exactly like those in the photoionization of the hydrogen atom. Similar to the $H^-$, the near-zero cross sections from the ionization threshold to a critical value of kinetic energy before the onset of fast-rising photoionization cross section is also clearly seen. Figure 7 presents the variation of the effective one-electron wave functions $\xi_p$ and their quasibound features for the outgoing ionized electron near the peak of the resonancelike structure with energies between 0.0601 and 0.0613 Ry at $D = 10a_0$. We should point out that the amplitude of the outside oscillating part of the radial wave function is noticeably smaller at $\epsilon = 0.0606$ Ry when the cross section is at its peak value. Although it appears that the resonancelike structure is similar to the usual Fano-Beutler autoionization resonance in the photoionization of plasma-free atoms, its nature is, nevertheless, different. The standard Fano resonance

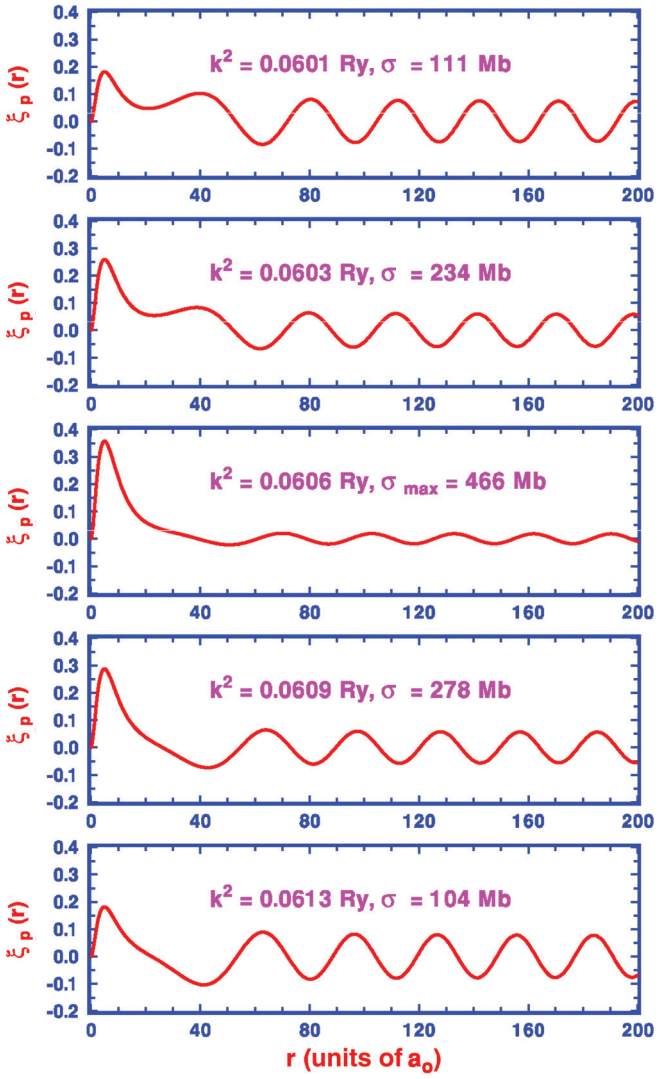


FIG. 7. (Color online) The variation of the effective radial wave functions $\xi_p$ of the outgoing ionized electron of He near the peak of the resonancelike structure with $A = 0$ and $D = 10a_0$.

is primarily due to the configuration interaction between the doubly excited bound state and the singly excited ionized channel [23]. In other words, it is the configuration mixing between two different types of two-electron configurations with different angular momentum combinations, i.e., different $\ell_1\ell_2$. The resonancelike structure in the photoionization of atoms in the plasma environment, on the other hand, is due to the mixing of bound and continuum components of the same angular momentum combination. Instead of a state function with the doubly excited bound component embedded in the singly ionized component with different $\ell_1\ell_2$ combination for the usual Fano resonance, what we have now is a state function with the singly excited quasibound component embedded in the singly ionized continuum component with the same $\ell_1\ell_2$ combination.

Figure 8 presents our theoretical results for He photoionization using the potential $V_s$ by Eq. (7) with a nominally chosen $A = 4a_0$. The vertical axis of the top plot is in logarithmic scale and the same spectra with the linear scale are shown in the bottom plot. Qualitatively, there is little difference in their

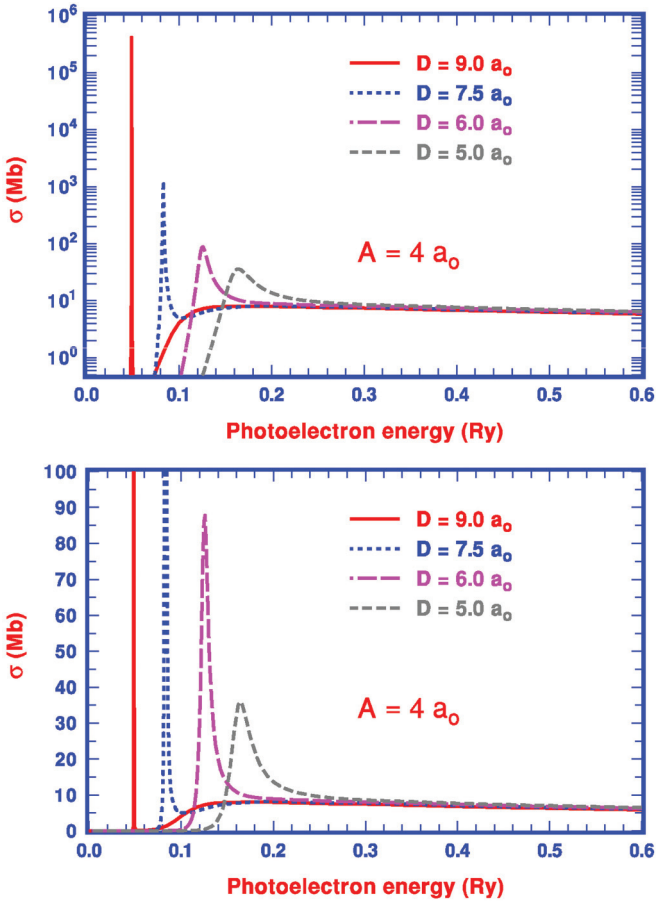


FIG. 8. (Color online) He photoionization spectra corresponding to $1s^2\,{}^1S \rightarrow 1s2p\,{}^1P$ transition with $A = 4a_0$ as $D$ varies.

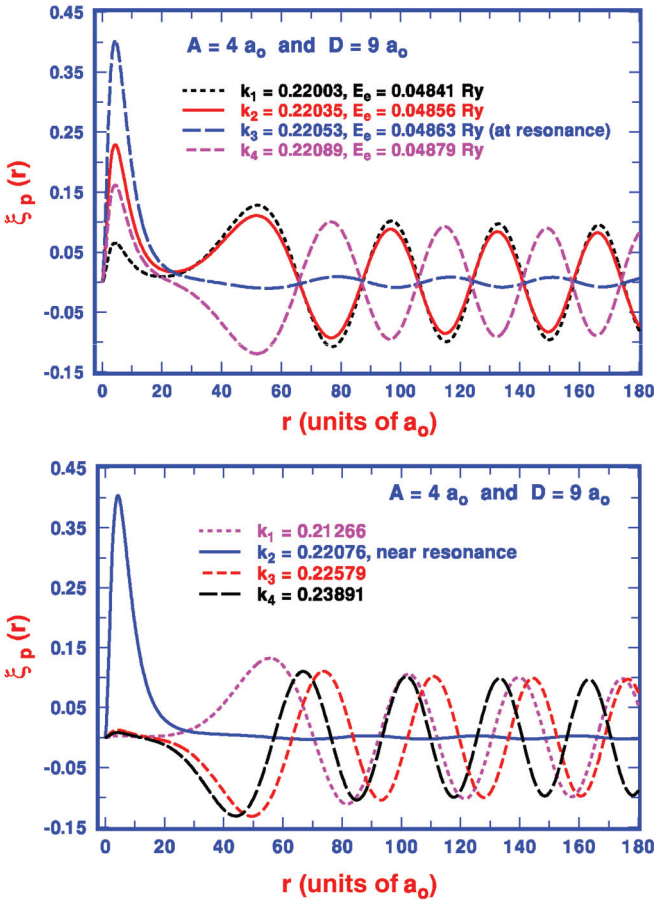


FIG. 9. (Color online) The variation of the effective radial wave functions $\xi_p$ of the outgoing ionized electron of He near the peak of the resonancelike structure with $D = 9a_0$ and $A = 4a_0$.

general features compared to the ones shown in Fig. 6 with $A = 0$, except the values of $D$ are chosen to be slightly smaller since the potential given by Eq. (7) is more attractive at $r \leqslant A$ for the same $D$. With $D = 9a_0$, the top plot of Fig. 9 shows that the magnitude of the innermost loop of the quasibound wave function of the outgoing electron at small $r$ rises up and falls down rapidly as energy changes by less than 0.0004 Ry with a center maximum at around $k = 0.22053$. It is interesting to note that the bottom plot of Fig. 9 shows a near-zero magnitude of the innermost loop of the wave functions of the outgoing electron at momenta on both sides but further away from $k = 0.22053$, due to the Coulomb repulsion from the remaining atomic electron as we discussed above. Since the photoionization cross section depends primarily on the overlap between the wave functions of the outgoing electron and the electron in its initial state, one could easily conclude, first, a narrow resonancelike spectrum, and second, near-zero cross sections from threshold until the quasibound nature appears in the wave function of the outgoing electron.

## IV. CONCLUSION

We present in this paper a detailed study of the photoionization of one- and two-electron atoms in a changing plasma environment based on the Debye-Hückel model. We have examined a number of general features of the photoionization spectra, including the common ones and also the distinctly different ones. For the one-electron hydrogenic system, we are able to link the photoionization spectra to the overlap between the wave functions of the outgoing ionized electron and the electron in its initial orbit or, more specifically, the dipole matrix for the transition. Since the atomic orbit of the electron in its initial state is usually limited to a small-$r$ region, the dynamics of the atomic photoionization from its ground state is short ranged in nature. For the two-electron atoms, we are able to carry out a similar analysis based on the configuration-mixed effective one-electron wave functions using the $B$-spline-based approach. We have concluded that the plasma-induced narrow resonance structures near the ionization threshold as the bound excited atomic states migrate into the continuum are due to the configuration mixing of quasibound and continuum components of the same $\ell_1\ell_2$ angular momentum combination in the state wave function. In other words, they are different in nature from the Fano-Beutler resonance, which is due to a state function with the doubly excited bound component embedded in the singly ionized component with different $\ell_1\ell_2$ combination. In addition, our calculation has led to a small but finite energy region with near-zero cross section starting from the ionization threshold in two-electron spectra. This near-zero cross-section window could be directly attributed to the presence of the second electron in the two-electron atoms. Finally, we would like to

point out that the redshifted narrow absorption resonances with large peak cross section such as the one shown in the bottom plot of Fig. 1 may offer the opportunity for observation with sufficient initial-state population and the currently available highly intense continuous light sources for the laser-produced plasmas similar to those already realized [17,18].

**ACKNOWLEDGMENTS**

This work was supported by the National Science Council in Taiwan under Grants No. NSC 100-2112-M-030-001 and No. NSC 102-2119-M-007-003. One of us (TNC) wishes to acknowledge a few in-depth discussions with Werner Däppen.

[1] A. N. Sil and P. K. Mukherjee, Int. J. Quantum Chem. **102**, 1061 (2005).
[2] P. K. Mukherjee, J. Karwowski, and G. H. F. Diercksen, Chem. Phys. Lett. **363**, 323 (2002).
[3] H. Okutsu, T. Sako, K. Yamanouchi, and G. H. F. Diercksen, J. Phys. B **38**, 917 (2005).
[4] S. B. Zhang, J. G. Wang, and R. K. Janev, Phys. Rev. A **81**, 032707 (2010); Phys. Rev. Lett. **104**, 023203 (2010); Y. Y. Qi, Y. Wu, J. G. Wang, and Y. Z. Qu, Phys. Plasmas **16**, 023502 (2009).
[5] C. Y. Lin and Y. K. Ho, Comput. Phys. Commun. **182**, 125 (2011); Eur. Phys. J. D **57**, 21 (2010).
[6] S. Sahoo and Y. K. Ho, J. Quant. Spectrosc. Radiat. Transfer **111**, 52 (2010); S. Kar and Y. K. Ho, *ibid.* **109**, 445 (2008); Phys. Plasmas **15**, 013301 (2008); Int. J. Quantum Chem. **106**, 814 (2006); A. Ghoshal and Y. K. Ho, J. Phys. B **42**, 075002 (2009).
[7] A. Ghoshal and Y. K. Ho, J. Phys. B **42**, 175006 (2009).
[8] Z. Wang and P. Winkler, Phys. Rev. A **52**, 216 (1995).
[9] S. T. Dai, A. Solovyova, and P. Winkler, Phys. Rev. E **64**, 016408 (2001).
[10] X. Lopez, C. Sarasola, and J. M. Ugalde, J. Phys. Chem. A **101**, 1804 (1997).
[11] F. J. Rogers, H. C. Graboske, Jr., and D. J. Harwood, Phys. Rev. A **1**, 1577 (1970).
[12] C. A. Rouse, Phys. Rev. **163**, 62 (1967).
[13] H. Margenau and M. Lewis, Rev. Mod. Phys. **31**, 569 (1959).
[14] P. Debye and E. Hückel, Phys. Zeitschr. **24**, 185 (1923).
[15] W. Däppen, Astrophys. Space Sci. **328**, 139 (2010).
[16] W. Däppen, J. Phys. A **39**, 4441 (2006); in *Solar and Stellar Physics Through Eclipses*, edited by Osman Demircan, Selim O. Selam, and Berahitdin Albayrak (Astronomical Society of the Pacific, San Francisco, CA, 2007), Vol. 370, pp. 3–12.
[17] Y. Leng, J. Goldhar, H. R. Griem, and R. W. Lee, Phys. Rev. E **52**, 4328 (1995).
[18] A. Saemann, K. Eidmann, I. E. Golovkin, R. C. Mancini, E. Andersson, E. Forster, and K. Witte, Phys. Rev. Lett. **82**, 4843 (1999); R. C. Elton, J. Ghosh, H. R. Griem, and E. J. Iglesias, Phys. Rev. E **69**, 067403 (2004).
[19] G. V. Marr, in *Photoionization Processes in Gases* (Academic Press, New York, 1967), p. 110.
[20] T. N. Chang, in *Many-Body Theory of Atomic Structure and Photoionization*, edited by T. N. Chang (World Scientific, Singapore, 1993), p. 213.
[21] T. N. Chang and T. K. Fang, Radiat. Phys. Chem. **70**, 173 (2004); Phys. Rev. A **52**, 2638 (1995); T. N. Chang and X. Tang, *ibid.* **44**, 232 (1991); T. N. Chang, *ibid.* **39**, 4946 (1989).
[22] K. Scheibner, J. C. Weisheit, and N. F. Lane, Phys. Rev. A **35**, 1252 (1987).
[23] U. Fano, Phys. Rev. **124**, 1866 (1961).